A 850-GHz Waveguide Receiver Employing a Niobium SIS Junction Fabricated on a 1-μm Si_3N_4 Membrane

Jacob W. Kooi, Jérôme Pety, Bruce Bumble, Christopher K. Walker, Henry G. LeDuc, P. L. Schaffer, and T. G. Phillips

***Abstract*— We report on a 850-GHz superconducting–insulator–superconducting (SIS) heterodyne receiver employing an RF-tuned niobium tunnel junction with a current density of 14 kA/cm^2, fabricated on a 1-μm Si_3N_4 supporting membrane. Since the mixer is designed to be operated well above the superconducting gap frequency of niobium ($2\triangle/h \approx 690$ GHz), special care has been taken to minimize niobium transmission-line losses. Both Fourier transform spectrometer (FTS) measurements of the direct detection performance and calculations of the IF output noise with the mixer operating in heterodyne mode, indicate an absorption loss in the niobium film of about 6.8 dB at 822 GHz. These results are in reasonably good agreement with the loss predicted by the Mattis–Bardeen theory in the extreme anomalous limit. From 800 to 840 GHz, we report uncorrected receiver noise temperatures of 518 or 514 K when we use Callen & Welton's law to calculate the input load temperatures. Over the same frequency range, the mixer has a 4-dB conversion loss and 265 K $\pm$10 K noise temperature. At 890 GHz, the sensitivity of the receiver has degraded to 900 K, which is primarily the result of increased niobium film loss in the RF matching network. When the mixer was cooled from 4.2 to 1.9 K, the receiver noise temperature improved about 20% 409-K double sideband (DSB). Approximately half of the receiver noise temperature improvement can be attributed to a lower mixer conversion loss, while the remainder is due to a reduction in the niobium film absorption loss. At 982 GHz, we measured a receiver noise temperature of 1916 K.**

***Index Terms*— Niobium superconducting film absorption loss, silicon–nitride membrane, SIS tunnel junction.**

I. Introduction

TO TAKE advantage of the 780–950-GHz atmospheric window for submillimeter astronomy, a full height waveguide superconducting–insulator–superconducting (SIS) heterodyne receiver with a center frequency of 850 GHz has been developed.

Manuscript received December 13, 1996; revised November 21, 1997. This work was supported in part under NASA Grant NAGW-107, and NSF Grant AST93-13929.

J. W. Kooi, J. Pety, P. L. Schaffer, and T. G. Phillips are with the Downs Laboratory of Physics 320-47, California Institute of Technology, Pasadena, CA 91125 USA (e-mail: kooi@tacos.caltech.edu).

B. Bumble and H. G. LeDuc are with the Center for Space Microelectronics Technology, Jet Propulsion Laboratory 302-231, California Institute of Technology, Pasadena, CA 91109 USA.

C. K. Walker is with Stewart Observatory, University of Arizona, Tuscon, AZ 85721 USA.

Publisher Item Identifier S 0018-9480(98)01591-9.

The results discussed here were achieved by using a 0.22-μm^2 Nb/AlO_x/Nb tunnel junction fabricated on a 1-μm Si_3N_4 membrane. The membrane is mounted on a pedestal, which is centered over a full-height rectangular waveguide. The mixer block is based on a design by Ellison *et al*. [1] and employs two circular noncontacting tuning elements [2], [3], magnetic-field concentrators [7], and an integrated 1–2-GHz IF matching network [14].

Traditionally, waveguide junctions have been constructed on quartz supporting substrates. To avoid RF leakage by means of surface modes down the quartz substrate, the cutoff frequency of these modes needs to be well above the operation frequency of the mixer. Unfortunately, the required thickness of the quartz and the dimensions of the substrate channel that hold the junction become unmanageably small for frequencies above 800 GHz. To avoid this problem, we explored the idea of fabricating the junction on a 1-μm Si_3N_4 membrane.

At the frequencies of interest, the photons have energies larger than the superconducting energy gap of niobium 2Δ and are able to break Cooper pairs within the superconductor. This results in a large absorption loss in the niobium transmission line situated in front of the mixer, thereby seriously degrading the receiver sensitivity. From the superconducting transmission-line theory [12], [16], we expect coupling efficiencies of about 30% with a $1/\sqrt{f}$ dependence. Detailed interpretation of the data confirm the $1/\sqrt{f}$ dependence; however, the observed loss appears to be about one-and-a-half times higher than the theoretically predicted loss. One possible explanation for the discrepancy is that based on the low current density in the niobium bowtie antenna and RF choke, we have assumed its loss negligible compared to the loss in the RF matching network. The loss in the RF choke could, however, be significant since it is critically dependent on the way the membrane is mounted in the junction block.

Independent from front-end loss calculations, we derive (using the pumped and unpumped *I–V* curves) a 3.9–5 dB double sideband (DSB) mixer conversion loss from 800 GHz to 1 THz, thereby demonstrating that the SIS junction is still a highly efficient mixing element well above the superconducting gap. The receiver response is thus only significantly limited by the absorption loss in the RF matching network. To improve on the sensitivity of the receiver, a better understanding of

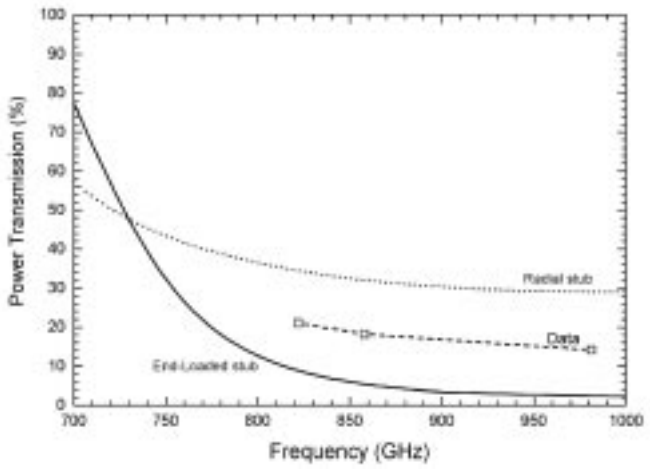

Fig. 1. Coupling efficiency calculations for both the radial and "end-loaded" stub matching networks (solid curves), and calculated efficiency from the heterodyne data (dashed line). A 9.3% RF reflection loss is included; however, the loss in the RF choke structure and bowtie antenna are not included in the simulated result.

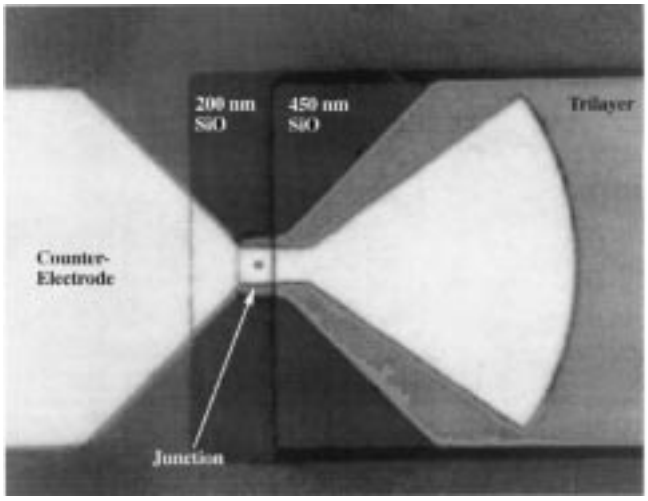

Fig. 2. 1000× photograph of the junction on silicon membrane. The transmission-line length is 2.5 μm on 450-nm SiO which is terminated by a radial stub with a fan angle of 70°. The junction size in the center of the bowtie antenna is 0.55 μm on a side.

higher Tc superconductor compound materials such as NbTiN or NbN and lower loss wiring materials such as Al and Au [17] is needed.

II. Junction Design

Above the gap frequency of niobium ($2\triangle/h \approx 690$ GHz), the photon energy is large enough to break Cooper pairs in the superconductor, causing large absorption loss in the niobium film. To minimize the absorption loss (calculated to be 50%–65% per wavelength at 850 GHz, depending on the SiO insulator thickness) in the RF tuning structure above the gap, it is important to keep the RF matching network as simple and short as possible. In Fig. 1, we compare the calculated coupling efficiencies of a radial stub and "end-loaded" stub RF matching network centered at 850 GHz [5], [6]. The "end-loaded" RF matching network typically employs two quarter-wave impedance transformer sections and a series inductive stub. The inductive stub is used to tune out the large junction susceptance, while the transformer provides a match to the much larger antenna impedance. Although the "end-loaded" stub matching network is successfully used with SIS devices below the gap frequency of niobium, above 700 GHz, wiring loss prohibits its use. For this reason we decided to use a radial stub RF matching network [9], [10]. It is interesting to note that this kind of matching network has a relative narrow bandwidth below the superconducting energy gap, while above it the frequency response will be broadened due to the dispersive loss in the niobium film.

The radial stub matching network functions by effectively placing an inductance, made out of a small section of niobium transmission line, in parallel with the junction (Fig. 2). In doing so, it resonates out the large parasitic junction capacitance of the junction ($\omega R_n C \approx 8.6$@850 GHz).

The loss in the niobium film (G_l) can be modeled as a conductance in parallel with the RF junction admittance $Y_{\rm rf}$, calculated from Tucker's theory [20]. For frequencies above that of the niobium gap, $Y_{\rm rf}$ is typically slightly less than G_n, the junction normal state conductance. The embedding impedance seen by the junction $Y_{\rm emb}$ in Fig. 3, thus includes a loss factor

$$G_p = \frac{G_l}{(1+Q^2)} \tag{1}$$

where G_l is the ohmic loss in the niobium film, Q the quality factor of the lossy RF matching network, and G_p the equivalent parallel conductance. In our case, $Q^2 \gg 1$ and (1) simplifies to

$$G_p \simeq \frac{B_l^2}{G_l} \tag{2}$$

where B_l is the shunt susceptance of the inductive transmission line. Power coupled to the junction is maximized by employing small area devices which decrease the transmission-line susceptance B_l. Secondly, the loss in the niobium can be decreased by maximizing the SiO insulating layer thickness to transmission-linewidth ratio (G_l maximized). In our case, we have opted for an insulator thickness of 450 nm, which is a standard process in the Jet Propulsion Laboratories–Micro-Device Laboratory (JPL–MDL) junction fabrication process. Lastly, by employing high current density devices we increase $Y_{\rm rf}$ by means of G_n, and thus increase the fraction of power coupled to the SIS device.

The properties of the superconducting microstrip lines are calculated using a method described by Zmuidzinas *et al*. [15]. The surface impedance is derived from the Mattis–Bardeen theory [16] in the extreme anomalous limit ($d \rightarrow \infty$ and $l \gg \delta$). Where d is the thickness of the niobium film, l the electron mean free path, and δ the penetration depth in niobium, ≈85 nm. Using a program written by Zmuidzinas and Bin, we find that given a 35-Ω probe impedance (Section III-B), optimum power transfer is obtained for a 70-Ω junction with a current density of ≈10 kA/cm^2. The actual device described in this paper has a current density of 14.2 kA/cm^2, area of 0.22 μm^2, and normal state resistance of 65 Ω.

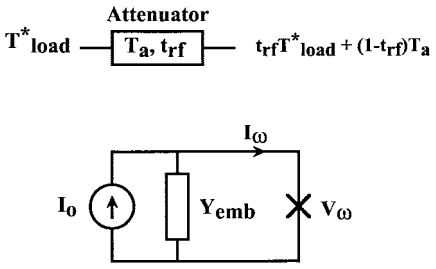

Fig. 3. RF port model used in our simulations.

In Section V-B, we find that the embedding impedance seen by the junction at 822 GHz is about $25.4 + j0.63\Omega$. Knowing $Z_{\rm emb}$, the junction capacitance and RF matching network parameters, we deduce an actual antenna impedance of $50.4 - j18\Omega$. Now using the actual rather than the theoretical 35-Ω antenna impedance in our computer model, we calculate a reflection loss at the RF port of 9.3%. The calculated loss in Fig. 1 was derived by correcting the RF transmission $t_{\rm rf}$ (Section V-B) for the front-end optics and RF matching network reflection losses.

III. Receiver Configuration

A. Mixer Block Construction

The front section of the mixer block is constructed on one mandrel in order to reduce the number of waveguide discontinuities and minimizes ohmic loss. It is composed of a corrugated feedhorn, circular-to-rectangular waveguide transformer and E-plane tuner. The Si_3N_4 membrane structure and circular noncontacting backshort tuner make up the back section of the mixer block. In our design, the E-plane tuner is situated $1/2\lambda_g$ in front of the junction and incorporates magnetic-field concentrators, as discussed by Walker *et al*. [7].

To further optimize the performance of the receiver, we have opted for the use of circular noncontacting E-plane and backshort tuners [2], [3]. These tuners consists of three beryllium–copper concentric circular sections that extend from a rectangular shaft which is carefully fit in the waveguide. The low- and high-impedance sections have diameters of 100 and 50 μm, respectively. Scale-model measurements have indicated that the position of the tuner in the waveguide is not critical as long as wall contact by the round sections is avoided.

On the IF side, the junction is wire bonded to the 1–2-GHz IF matching network [14], and the mixer block ground (Fig. 3). The matching network is designed to transform a 160-Ω IF impedance to 50 Ω and to provide a short to out-of-band signals up to $\approx$22 GHz to avoid saturating the junction with unwanted out-of-band signals. The output of the mixer block is directly connected to a cryogenic cooled 1–2-GHz balanced high electron mobility transistor (HEMT) amplifier based on work by Padin *et al*. [8]. Reflections caused by the impedance mismatch between the matching network and low-noise amplifier are partially absorbed by the amplifier's input Lange coupler ($S11 \leq -10$ dB).

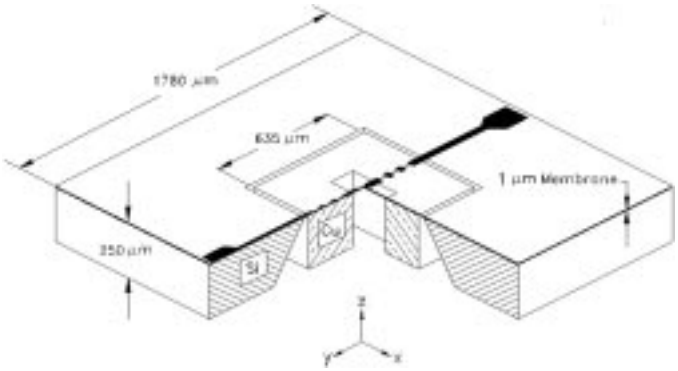

Fig. 4. Rendering of the 1-μm Si_3N_4 membrane, RF choke, and silicon support structure that houses the SIS tunnel junction and RF matching network.

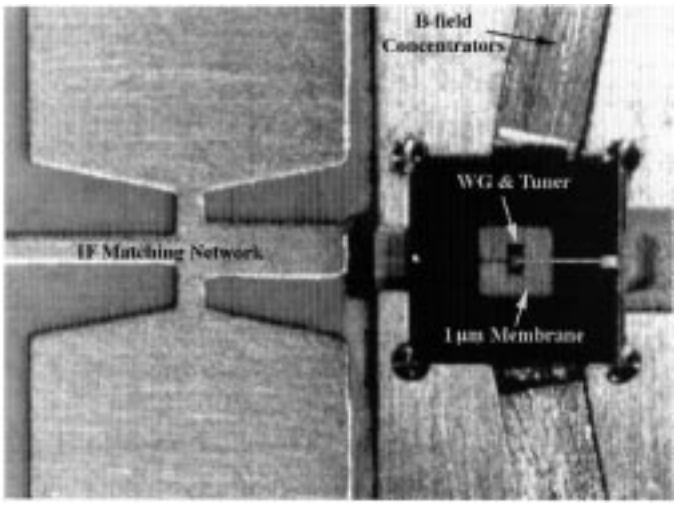

Fig. 5. View of the silicon–nitride membrane situated in the mixer block. The membrane extends 50 μm over the pedestal for stress relief. Looking through the membrane, one sees the waveguide (250 μm $\times$ 125 μm) and outline of the circular tuner low-impedance section (100 μm diam., about twice the size of a human hair).

B. Membrane Construction

Fig. 4 depicts the Si_3N_4 membrane situated on top of a copper pedestal which houses the waveguide. The membrane itself is supported by silicon etched along the 111 crystal plane.

The membrane was placed on top of an optically polished flat copper pedestal which provides the ground plane for the microstrip-mode RF choke (Fig. 5). A 100-μm groove has been machined in the mixer horn block directly above the RF choke. The RF choke structure on top of the membrane provides a short circuit at the waveguide wall when the bowtie antenna and RF matching network are centered in the waveguide.

Perhaps a better design incorporates a suspended RF stripline, which provides dimensional freedom in the Z-direction. A 2–3-μm polymethyl methacrylate (PMMA) spacer is placed between the junction block housing the membrane and the horn block to prevent the membrane from breaking when the two blocks are fit together in the final mixer assembly. The devices are glued into a "moat" by means of a 50% solution of nail polish (polyester resin) in butylacetate.

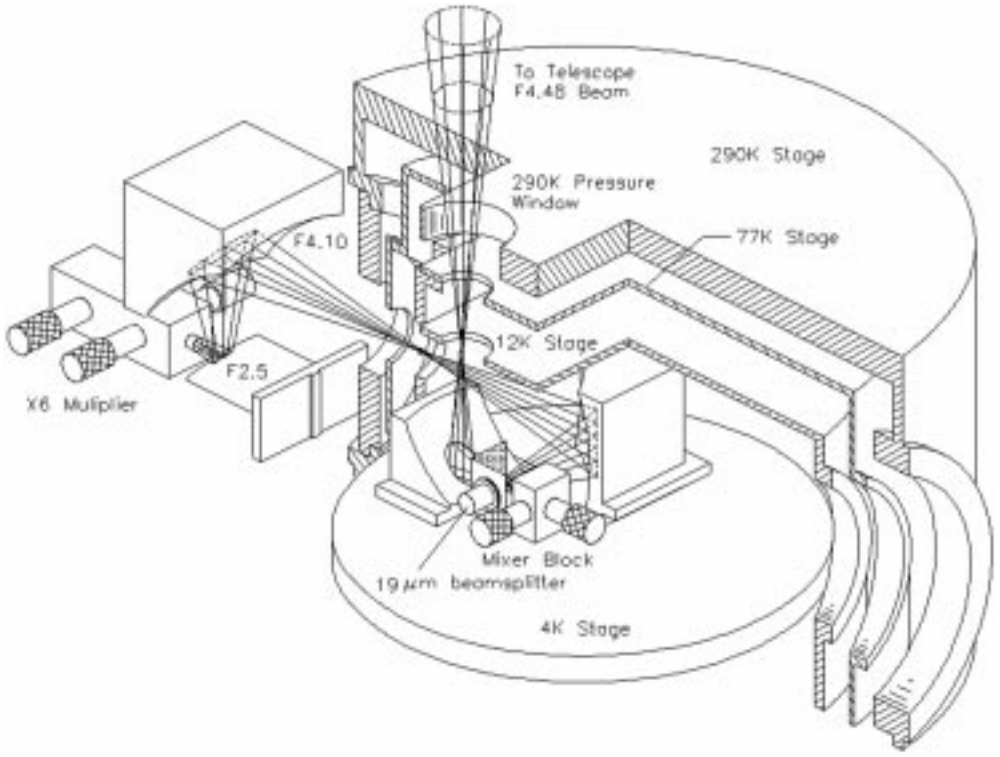

Fig. 6. Isometric cutaway view of the optics configuration employed. The cryostat is mounted upside down in the Cassegrain focus of the Caltech Submillimeter Observatory (CSO).

Securing devices this way has the advantage that they are easily removed with acetone, yet cycle securely to LHe temperatures. As far as we can tell, *I–V* characteristics of both LHe dipped junctions and those cooled in a vacuum dewar are identical. This is a good indication that the thermal conductivity of the silicon–nitride membrane is high enough to prevent heating of the junction by infrared (IR) radiation.

To obtain a better understanding of the probe impedance of the bowtie antenna on top of the silicon–nitride membrane mounted in the mixer block (see Fig. 3), we performed a series of scale-model measurements. From it we determined an embedding impedance of about 35 Ω, and have made the assumption in our computer simulations that this impedance is fixed (by adjusting both E-plane and backshort tuner accordingly).

C. Cooled Optics

The receiver noise temperature is critically dependent on $t_{\rm rf}$, defined as the combined front-end optics and niobium film transmission coefficient

$$T_{\rm rec} = \frac{(T_{\rm rf} + T_{\rm mix} + T_{\rm IF})}{t_{\rm rf} G_{\rm mix}^{\rm DSB}}. \tag{3}$$

$G_{\rm mix}^{\rm DSB}$ is the mixer gain and $T_{\rm rf}$, $T_{\rm mix}$, $T_{\rm IF}$ are the front-end mixer and IF noise temperatures referred to the output of the mixer.

From the point of view of optimizing the receiver performance, we tried to maximize $t_{\rm rf}$ by carefully selecting the IR blocking filters and eliminating the use of plastic lenses in the optics path. Furthermore, to minimize the noise contribution from the 12% reflective mylar beamsplitter, we decided to combine the RF and local oscillator (LO) power on the LHe stage. Fig. 6 shows an isometric view of the optics configuration.

The corrugated feedhorn beamwidth was measured by Walker *et al*. on a scaled version at 115 GHz. It measures 10.5° at the ε^{-2} power contour in both E- and H-plane. This beam is transformed by means of an off-axis ellipsoidal mirror to an F4.48 beam with a 12-dB edge taper at the secondary mirror of the telescope (Fig. 6). Both LO and RF beams have their second foci between the 12- and 77-K stages of the cryostat. This allows the use of 40-mm-diam. 2.5-mm-thick crystal quartz pressure windows.[1] The IR blocks on the 77-K stage are made out of 1.25-mm-thick crystal quartz disks, 25 mm in diameter. The quartz lenses are antireflection coated with clear Teflon $(n = 1.44)$.[2] At the 12-K stage, we use a 30%–60% porous 190-μm-thick Teflon sheet[3] to scatter the remaining IR photons. Fourier transform spectrometer (FTS) transmission measurements of the Teflon antireflection coated crystal quartz lenses indicate a 95%–97% transmission efficiency in the submillimeter range. Heterodyne transmission measurements of the Zitex porous teflon material[3] at 822 GHz give 99% transmission per sheet, while spectrometer measurements in the near IR (10 μm) show a 98.5% loss per sheet, due to scattering of the IR photons.

Outside the dewar, the LO beam is refocused via a 45° flat mirror to match the waist of the 780–870-GHz multiplier

[1] Valpey–Fisher (Subsidiary of Matec), Hopkinton, MA, 01748 USA.

[2] Thermech Engineering Corporation, Anaheim, CA 92801 USA; Francis Lord Optics, Gladesville, N.S.W. 2111, Australia.

[3] Norton Performance Plastics, Wayne, NJ 07470 USA.

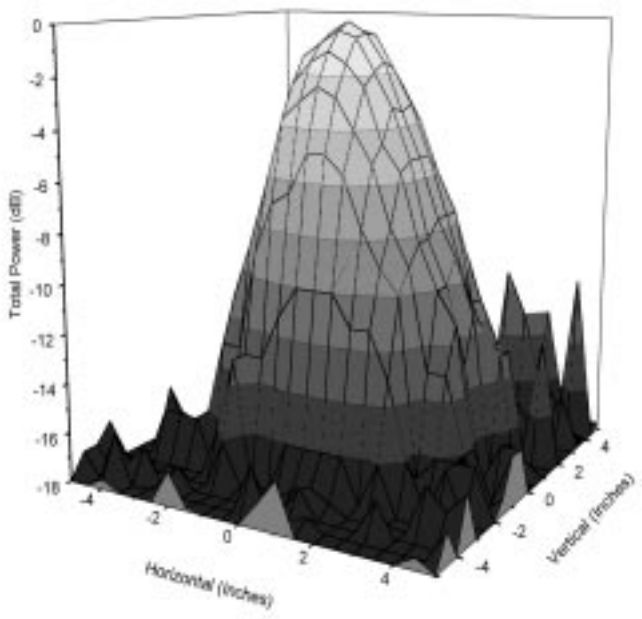

Fig. 7. Far-field pattern of the receiver beam measured at 822 GHz. The beam matches the F4.48 telescope beam and has a 12-dB edge taper on the chopping secondary mirror.

[13]. To help avoid standing waves between the secondary and the instrument, the vacuum windows and IR blocks were tilted at 5° angles. The receiver performance has been carefully measured with both the cooled beamsplitter/mirror and warm beamsplitter/cooled lens combination. All other hardware being the same, we noted an 75-K reduction in receiver noise temperature when using the cooled beamsplitter/mirror configuration. Analyses of the data show that this is primarily due to the elimination of reflection loss of the 4-K low-density polyethelene lens, e.g., $t_{\rm rf}$ improved by about 8%.

To investigate the far-field beam (see Fig. 7) characteristics of the waveguide mixer, an antenna beam test stand was employed. The measurement technique involves using a lock-in amplifier to detect a chopped hot-load/cold-load signal source, while the source is moved normal to the E- and H-plane of the antenna beam. The hot load is a grooved piece of macor, attached to a heating element. The cold load is room-temperature Eccosorb. The signal source is aperture limited, approximating a point source in the far field.

IV. Nb/AlO_x/Nb Junction and Chip Fabrication

Devices are fabricated on (100) oriented silicon wafers which are 254-μm thick, 51-mm diam., and polished on both sides. The Si_3N_4 is grown under conditions for reduced stress by low-pressure chemical vapor deposition (LPCVD) to a thickness of 1 μm. Fabrication of the Nb/AlO_x/Nb tunnel junction is accomplished using a standard trilayer deposition technique [18], [19]. Magnetron sputter deposition and room-temperature oxide growth are done *in situ* in an ultrahigh vacuum system with a base pressure of 2×10^{-9} torr.

The trilayer is deposited by a lift-off process employing a multilayer photolithographic technique using PMMA under AZ5214 photoresist. This step forms one side of the antenna/filter structure with layers of 160-nm Nb base, 6-nm Al, and 90-nm Nb counter-electrode.

A junction mesa of 0.3-μm^2 area is defined by direct-write-electron beam lithography in a 100-nm-thick PMMA stencil. Chromium is deposited through the PMMA stencil and serves as an etch mask over 500 nm of polyimide. Contact regions of the trilayer are then protected by adding a photoresist stencil. The combined chromium + photoresist/polyimide structure is etched using an oxygen reactive ion etch (RIE). Polyimide remaining defines an isolation window and junction mesa for subsequent Nb RIE. To achieve Nb etch directionality, we utilize a gas mixture of 62% CCl_2F_2 + 31% CF_4 + 7% O_2. Electrical isolation of the base electrode from the wire layer is provided by thermal evaporation of 200 nm of SiO. Samples are rotated at a slight tilt angle during SiO deposition to assure both good isolation and self-aligned lift-off with the polyimide. Lift-off is done by dissolving the polyimide in dichloromethane. A subsequent photoresist pattern is used to produce a total SiO thickness of 450 nm under the tuning stub element only. The second half of the antenna/filter is formed by a blanket deposition of 250-nm Nb capped with 30-nm gold for contacts. RIE etching with an AZ5206 photoresist stencil defines this final frontside pattern. Window openings are patterned on the backside by IR alignment to the front. This step is masked with AZ5218 photoresist which enables CF_4 + 19% O_2 RIE etching through the backside Si_3N_4.

Exposed silicon areas on the backside are anisotropically etched in a bath of 30% KOH solution at 70 °C. Etching stops after about eight hours, when only the frontside membrane and side (111) silicon planes are left exposed. The devices on the front are protected from the KOH solution by an "O"-ring enclosure. A layer of wax on the device side also helps localize wafer damage if one of the Si_3N_4 windows happens to break during KOH etching. Individual chips 1.78 mm × 1.78 mm are diced from the wafer using a diamond saw.

Device yield with this process is typically lower than similar devices which we make on either Si or quartz substrates. We have not determined exactly how to increase yield; however, many devices with current densities of about 12 kA/cm^2 and subgap to normal state resistance ratios of greater than ten have been fabricated on multiple wafer runs.

V. Receiver Performance

A. FTS Measurements

To measure the response of the RF matching network, we have tested junctions as direct detectors using an FTS. The devices have been mounted quasi-optically against a quartz hyperhemispherical lens, as described by Büttgenbach *et al.* [4]. The advantage of this method is that there are no external tuning elements in the system, as in the case with a waveguide mount and, as such, the overall frequency response of the junction can be measured.

The disadvantage is that the junction's bowtie antenna and RF choke are mounted slightly out of focus on the back of an hyperhemispherical lens. This presents an unknown and

frequency-dependent embedding impedance, which affects the magnitude of the video response.

Compared to FTS measurements on 665-GHz tuned junctions, the response of the 850-GHz tuned junctions on silicon–nitride membrane has degraded ≈4–7 dB. This is in fairly good agreement with the absorption loss predicted by the Mattis–Bardeen theory. Because of the many uncertainties in the optics of these quasi-optically mounted waveguide junctions and the quality of the junctions, it is not possible to quote a more precise number.

The measured response is shifted down in frequency, compared to design, by about 50 GHz, or 6% [11].

B. SIS Simulations

To simulate the receiver response to a cold or hot load, we used a three-port model, as described by Tucker and Feldman *et al*. [20]. In our simulations, all the harmonic sidebands are assumed to be shorted by the parasitic junction capacitance. Moreover, the receiver is assumed to work in a true DSB mode, which means that the embedding admittance seen by the junction is identical at the upper sideband (USB), lower sideband (LSB), and LO frequencies. This way, the two RF ports can be described by a single circuit. To use this theory, we first find the RF and IF embedding admittance.

Fig. 3 shows the RF port model which we divide into an attenuator stage and a lossless RF circuit. The attenuator takes into account the front-end optics loss and absorption loss in the niobium film of the tuning circuit. The lossless RF circuit is described as a current source I_0 whose admittance $Y_{\rm emb}$ is the embedding admittance seen by the junction.

The embedding admittance is deduced from a solution of the lossless RF circuit equation

$$I_{\rm LO} = Y_{\rm emb} \cdot V_w + I_w(V_{\rm dc}, V_w) \tag{4}$$

where the RF junction current (I_w) is computed from the unpumped *I–V* curve and its Kramers–Kronig transform [20, eq. (4.40), (4.41)]. Following Skalare [24], we first find the RF junction voltage ($V_w^k = \alpha^k \hbar\omega/e$) at each point k of the pumped *I–V* curve ($V_{\rm dc}^k$). With this set of points (all belonging to the first photon step), we are now able to find the parameters $|I_{\rm LO}|$ and $Y_{\rm emb}$, which minimize the function

$$\sum_k \left| |I_{\rm LO}|^2 - \left| Y_{\rm emb} \cdot V_w^k + I_w\left(V_{\rm dc}^k, V_w^k\right)\right|^2 \right|. \tag{5}$$

At 822 GHz, we found $Z_{\rm emb} = 25.4 + j0.63\Omega$ and $|I_{\rm LO}| = 132.3$ μA. Once $Y_{\rm emb}$ and $|I_{\rm LO}|$ are known, we can compute the pumped *I–V* curve (Fig. 8) and compare it with the measured data.

Fig. 9 shows the IF port model. Here, the IF chain includes the matching network [14] and the IF amplifier. To characterize the IF noise contribution, Rudner and Feldman [21], and Woody, Miller, and Wengler [22], proposed to use the unpumped junction above the gap voltage as a calibrated shot noise source. Two recent studies by Dubash *et al*. [25], [26] quantitatively verified that the noise current of an unpumped SIS junction is, in fact, the shot noise associated with the direct current. Using this study, Woody *et al*. [28] used the IF output

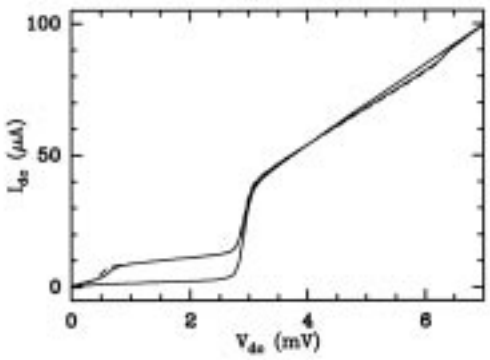

Fig. 8. Measured and calculated pumped and unpumped *I–V* curves. The optimum bias appears to be 2.25 mV with a pumped LO current of 8.5 μA, which corresponds to $\alpha \equiv eV_w/\hbar\omega = 0.75$. The junction has a resistive subgap to R_n ratio of ≃10.

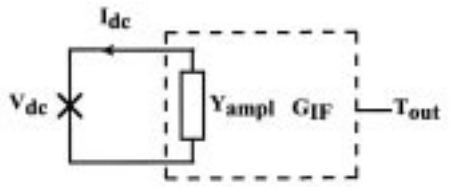

Fig. 9. IF port model.

power response of the unpumped mixer over the full *I–V* curve to completely characterize the IF chain.

To do so, they used the standard IF noise temperature [23] which is

$$T_{\rm IFO} = T_{\rm min} + T_d \frac{|Y_{\rm opt} - Y_s|^2}{G_s G_{\rm opt}} \tag{6}$$

where $Y_s = G_s + jB_s$ is the input source admittance, $T_{\rm min}$ the minimum noise temperature, $Y_{\rm opt} = G_{\rm opt} + jB_{\rm opt}$ the source admittance that achieves this minimum, and T_d a measure of the noise sensitivity to deviations from $Y_{\rm opt}$. This analysis allows a fit to the IF output power of the unpumped mixer using the model

$$P_{\rm out} = g_{\rm IF} G_{\rm ampl} B \frac{2eI_{\rm dc}^{\rm unpumped} + 4kT_{\rm IFO}G_s}{|Y_{\rm ampl} + Y_s|^2}. \tag{7}$$

Here $Y_{\rm ampl} = G_{\rm ampl} + jB_{\rm ampl}$ is the input admittance of the IF chain terminated by a 50-Ω load, $g_{\rm IF}$ the total IF gain, Y_s the IF output admittance of the junction, and B the IF bandwidth. To fit to the measured IF output power, we have to rewrite (7) as

$$P_{\rm out} = g \frac{2eI_{\rm dc} + aG_s^2 + bG_s + c + dB_s}{|Y_{\rm ampl} + Y_s|^2} \tag{8}$$

where g, a, b, c, d, defined in Woody's paper, are combinations of $g_{\rm IF}$, B, $T_{\rm min}$, T_d, $Y_{\rm opt}$, and $Y_{\rm ampl}$.

Our experience is that the fitting procedure has two shortcomings. First, it can not distinguish between a large range of values for $Y_{\rm ampl}$. To overcome this problem, we fixed $Z_{\rm ampl}$, well known from network measurements, to 160 Ω [14].

TABLE I
RANGE OF ACCESSIBLE FITTING VALUES AT 822 GHz

Parameter	Range
T_{min} (K)	0.12 – 5.98
T_d (K)	2.74 – 5.66
R_{opt} (Ω)	76.69 – 155.5
X_{opt} (Ω)	-137.1 – -22.89

Secondly, for SIS heterodyne receivers, the mixer IF output susceptance is negligible (while the conductance is simply equal to the derivative of the *I–V* curve). Due to this fact, the fitting procedure cannot give the value of d, which prevents us from finding the exact values of $T_{\min}$, T_d, and $Y_{\rm opt}$. We only are able to determine a range of values (see Table I). Knowing that a reasonable minimum IF noise temperature is ≈5 K, we obtain $T_d \simeq 5.2$ K, $R_{\rm opt} \simeq 145\,\Omega$, and $X_{\rm opt} \simeq -61\,\Omega$. While the actual physical values are difficult to find with precision, the fitting parameters are very well constrained by the data. This allows us to compute with good precision the IF noise contribution to the total output power as a function of the direct bias voltage for the pumped mixer. We only need to replace $I_{\rm dc}^{\rm unpumped}$ by $I_{\rm dc}^{\rm pumped}$ in (8).

Using the Tucker theory [20] in the low IF approximation, we can then compute the DSB mixer gain $G_{\rm mix}^{\rm DSB}$, and the noise power at the mixer output $T_{\rm mix}$ (see Table II). The downconverted quantum noise at the mixer output is computed as explained by Wengler and Woody [27]. Finally, the RF attenuator (Fig. 7) is characterized by a transmission factor $t_{\rm rf}$ and a noise temperature T_a. $t_{\rm rf}$ and T_a can be found by adjusting the computed hot and cold total IF output power to fit the data. At 822 GHz, $t_{\rm rf} = 0.146$ (−8.3 dB) and $T_a = 22.1$ K. Given these values, we compute an available LO power of 427 nW.

Fig. 10 shows the total output power (bottom panel) as well as the decomposition in its different parts as a function of the bias voltage. All the simulated powers (in temperature units) are the powers dissipated in the IF matching network input admittance $(Y_{\rm ampl})$. The mixer and IF noise temperatures $T_{\rm mix}$ and $T_{\rm IF}$ thus include the mismatch between the junction and the IF matching network. $T_{\rm IFO}$ used in (6) will be linked to $T_{\rm IF}$ by $T_{\rm IF} = \Gamma_{\rm IF} T_{\rm IFO}$ where

$$\Gamma_{\rm IF} = \frac{4G_sG_{11}}{|Y_{\rm ampl}+Y_s|^2} = 0.83 \qquad \text{at } 2.25 \text{ mV}. \tag{9}$$

In Fig. 10, the dashed curves are the results for the cold load while the solid curves are the results for the hot load. Because the photon energy is larger than the gap frequency of niobium, the photon step overlap from the negative part of the *I–V* curve (not shown here) partially cancels the photon step from the positive part of the *I–V* curve. In the top panel, we show the noise produced by the hot or cold loads at the input $t_{\rm rf}G_{\rm mix}^{\rm DSB}T_{\rm load}^{*}$. In the text, * indicates that the input load is defined using the Callen and Welton formula [31], [32] which gives, for the hot and cold load, 297.4 and 81.6 K, respectively. This is opposed to an uncorrected hot and cold load temperature of 297 and 80 K in the Rayleigh–Jeans limit, as is common practice for lower frequency receivers. The emissivity of the cold load is estimated to be about 98%.

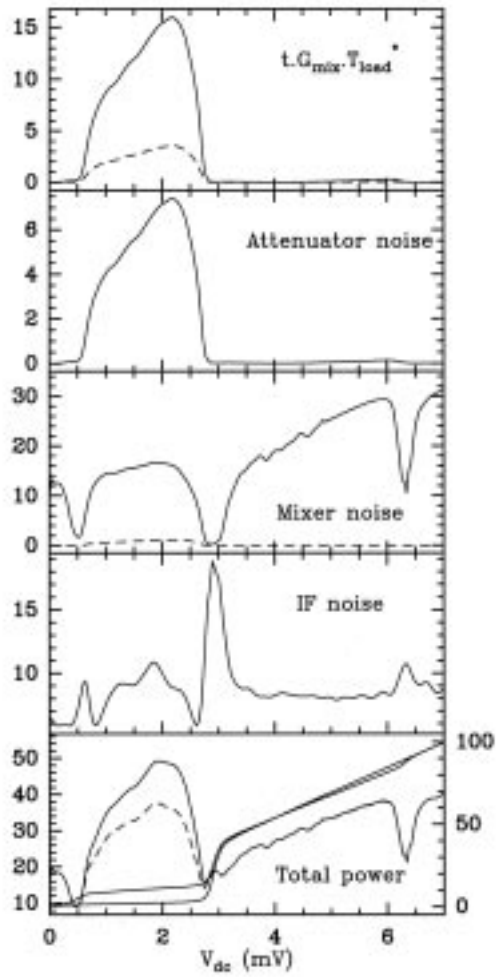

Fig. 10. Composition of the receiver output power at 822 GHz. Powers (left axis) are given in temperature units while the *I–V* curves (right axis) are in μA.

The second panel from the top shows the attenuator noise contribution $G_{\rm mix}^{\rm DSB}(1-t_{\rm rf})T_a$. In the third panel, we plot the mixer output noise power, which is made up of the shot noise in the mixer plus the quantum noise. The quantum noise, which is the absolute receiver noise limit, is shown as the dashed curve. The fourth curve is the IF noise contribution while the remaining curve is the total power, the sum of all the above curves.

C. Heterodyne Results and Discussion

The 822-GHz measured and calculated hot and cold total power response is shown in Fig. 11(a). The Shapiro steps were carefully suppressed by adjusting the magnetic field. In Fig. 11(b), we show the measured and calculated Y factor (total power ratio). Note the good agreement between theory and measurement.

Table II tabulates the measured and simulated receiver parameters at 822 GHz. Using the intersecting line technique described by Blundell, Ke, and Feldman *et al.* [29], [30], we derive a corrected front-end noise temperature of 154 K*. This compares to a simulated front-end noise temperature of

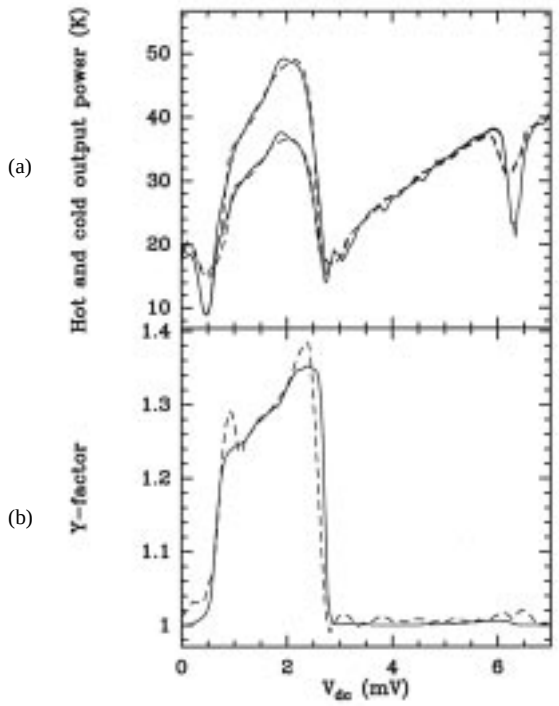

Fig. 11. Total power response at 822 GHz. The optimum receiver noise temperature at 822 GHz was 514 ± 5 K DSB. At 1.9 K ambient temperature, the corrected receiver noise temperature improved to 409 K DSB. The solid curves are the data, while the dashed lines are the simulated results.

TABLE II
MEASURED AND CALCULATED RECEIVER PARAMETERS AT 822 GHz FOR $V_{dc} = 2.25$ mV AND $\alpha = 0.75$

Parameters	Data*	Simulation*
Trec (K)	514	514
$T_a(1-t_{rf})/t_{rf}$ (K)	154	129
T_{mix} (K)	13.72	14.67
T_{IF} (K)	6.23	8.0
G_{mix}^{DSB} (dB)	–	-4.0
$t_{rf}G_{mix}^{DSB}$ (dB)	-12.57	-12.3
$T_{mix}/(t_{rf}G_{mix}^{DSB})$ (K)	248	249
$T_{IF}/(t_{rf}G_{mix}^{DSB})$ (K)	112	136

129 K. Caution must be taken when directly comparing these results. The intersecting line technique is likely to include some small correction factors (τ) because the mixer is not perfectly matched and/or operating in true DSB mode [30]. The magnitude of τ is some fraction of $\hbar\omega/k = 39.5$ K at 822 GHz.

Using the Shot noise method [21], [22], we calculate an overall mixer conversion gain of −12.6 dB, mixer noise temperature of 248 K, and IF noise temperature (as referred to the output of the mixer) of 6.2 K. These results are in good agreement with the simulation where we are able to separate the total front-end loss (8.3 dB) from the actual mixer down-conversion loss (4 dB). From FTS measurements, we estimate a total front-end optics loss of 1.1 dB and an RF mismatch of ≈0.42 dB (Section II). This leaves a niobium absorption loss of about 6.8 dB (79%), due to the antenna, choke, and RF matching network. The calculated loss compares favorably with earlier FTS measurements [11], and is about one-and-a-half times the loss expected from the Mattis–Bardeen theory (65.4%).

TABLE III
MEASURED AND CALCULATED RECEIVER PARAMETERS FOR DIFFERENT FREQUENCIES AND AMBIENT TEMPERATURES

Parameters	822 GHz at 1.9K	858 GHz at 4.2K	982 GHz at 4.2K
Trec* (K)	409	577	1916
$T_a(1-t_{rf})/t_{rf}$ (K)	86	137	254
T_{mix} (K)	11.7	11.5	12.37
T_{IF} (K)	12.0	10.5	8.5
G_{mix}^{DSB} (dB)	-3.5	-3.9	-5.0
$t_{rf}G_{mix}^{DSB}$ (dB)	-11.3	-13.0	-19.1
$T_{mix}/(t_{rf}G_{mix}^{DSB})$ (K)	159	230	1006
$T_{IF}/(t_{rf}G_{mix}^{DSB})$ (K)	164	210	656
V_{gap} (mV)	2.9	2.8	2.8

When the mixer was cooled from 4.2 to 1.9 K, the receiver noise temperature improved about 20% to 409 K DSB (see Table III). Interpretation of the measurements show that $G_{\rm mix}^{\rm DSB}$ increases about 12% to −3.5 dB, which is similar to what is observed below the gap [3]. This can be attributed to the sharpening of the *I–V* curve. An additional 12.2% improvement in the front-end transmission $t_{\rm rf}$ is gained as the result of a slightly higher energy gap (≈2.9 mV), and, therefore, reduced loss in the niobium film.

At 858 GHz, we calculate a DSB mixer down-conversion loss and front-end loss of 3.9 and 9.1 dB, respectively. Of the 9.1 dB, about 1.2 dB is due to loss in the optics, while another ≈0.5 dB is caused by reflection loss of the RF matching network. The calculated niobium film transmission loss at 858 GHz is, therefore, ≈82%, as opposed to a theoretically expected loss of 68%.

At 982 GHz, the DSB mixer conversion gain has degraded to about −5 dB, which comes as no surprise since we are tuned away from the resonant peak. The front-end reflection loss at this frequency is about 1.8 dB, so that we have a niobium transmission loss of 87% (8.8 dB), assuming in this case a RF reflection loss of 0.5 dB.

From this discussion, it is clear that the niobium SIS junction is still a highly efficient mixing element up to at least 1 THz (2.9Δ) [33], but that the loss in the niobium film is severely limiting the receiver sensitivity (Fig. 1). Given the performance of the mixer, receiver noise temperatures as low as 250–300-K DSB at 1 THz should be achievable with a higher T_c (≥14 K) superconducting materials such as NbTiN.

The measured frequency response of the 850-GHz receiver at both 4.2 and 1.9 K is shown in Fig. 12. At 982 GHz, the sensitivity has degraded to 1916-K DSB, which is primarily due to the loss in the niobium tuning circuit. In all circumstances, the receiver was tuned for maximum IF power, which occurs when $G_{\rm mix}^{\rm DSB}$ is optimized.

VI. OBSERVATIONS

In December 1996, we observed ^{12}CO $J = 7 \rightarrow 6$ (807 GHz) and detected atomic carbon Cl $2 \rightarrow 1$ (809 GHz) in the Orion bar region at the CSO (see Fig. 13). System temperature and total integration time were ∼4400 K and 47 min, respectively. The main beam efficiency measured

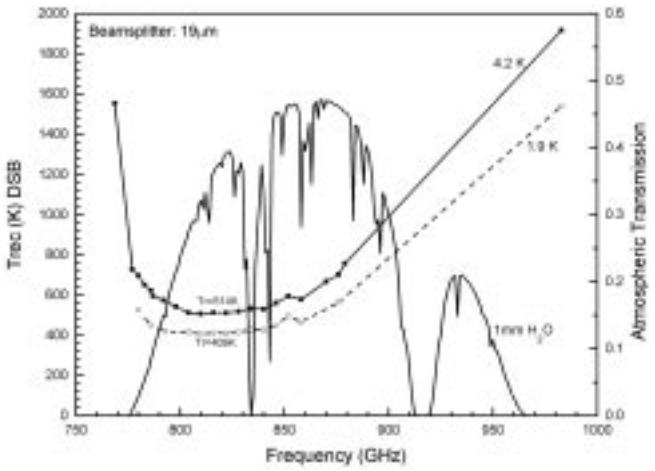

Fig. 12. Frequency response of the 850-GHz waveguide receiver discussed. The receiver employs a radial stub RF matching network and two mechanical circular tuners. When installed at the CSO, the receiver noise temperature improved 8% (475 K @ 809 GHz) across the band, which is attributed to the lower LHe bath temperature (3.55 K) at the 4200-m altitude site.

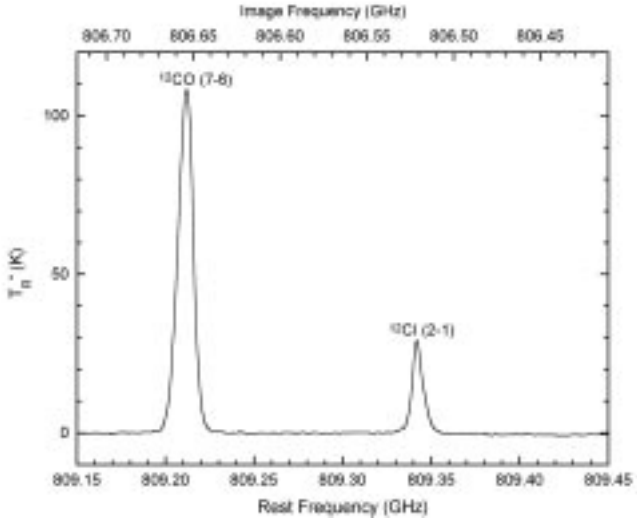

Fig. 13. A spectrum of the Orion bar in ^{12}CO $J = 7 \rightarrow 6$ and Cl $2 \rightarrow 1$, taken at the CSO.

on Mars (10 arcsec diam.) was 33%, while the approximate zenith atmospheric transmissions was 40%. The spectrum was corrected for an estimated extended source coupling efficiency of 60%.

VII. Conclusion

We have discussed the design and development of a 850-GHz waveguide heterodyne receiver employing a tuned 0.22-μm^2 Nb/AlO$_x$/Nb SIS tunnel junction on a 1-μm silicon–nitride membrane. The membrane is mounted on a copper pedestal with the bowtie antenna centered on the waveguide. To take advantage of the accuracy that can be achieved with silicon micromachining, it is recommended that for future terahertz applications, a micromachined waveguide mount and suspended stripline membrane design be combined.

We have demonstrated the effectiveness of the radial stub RF matching network to tune out the large parasitic junction capacitance and minimize the absorption loss of the niobium film above the superconducting energy gap of niobium.

Direct detection response measurements with a FTS indicate response from 700 to 1100 GHz, which are confirmed by Josephson resonances in the *I–V* curve. Calculations of the niobium absorption loss on the measured heterodyne data confirms the expected $1/\sqrt{f}$ dependence. Both heterodyne and direct detection response measurements give a loss one-and-a-half times higher than predicted by the Mattis–Bardeen theory. Although the origin of the excess loss is not completely clear, it is important to note the generally good agreement with the theory.

From 800 to 840 GHz, we report corrected receiver noise temperatures of 514-K DSB in the laboratory and 475-K DSB at the Observatory due to the lower LHe bath temperature at the high elevation. Over the same frequency range, we calculate a DSB mixer conversion gain of about -4 dB, a mixer noise of $\approx$265 K, and a front-end loss of $\approx$130 K. At 890 GHz, the sensitivity has degraded to 900 K, which is primarily a result of the increased loss in the niobium film. Cooling the mixer to 1.9 K, the receiver noise temperature from 790 to 840 GHz improved about 20% due to a slightly higher and sharper niobium energy gap. The receiver response is clearly limited by the absorption loss in the RF matching network, and to improve the sensitivity of the receiver, a better understanding of higher Tc superconductor compound materials such as NbTiN or NbN and lower loss wiring materials such as Al and Au are needed.

Acknowledgment

The authors wish to thank Prof. J. Zmuidzinas, M. Bin, R. Schoelkopf, B. Chan, J. Ward, T. Hunter, T. Kerr, and M. Feldman for helpful discussions, K. Young, J. Keene, and D. Lis for help with the observations, Prof. Y.-C. Tai and his group at Caltech for the silicon–nitride deposition, D. Miller for help with the optics measurements, D. Tahmoush and D. Benford for help with the IR transmission and reflection measurements, K. Horvath for his superb craftsmanship on making the mixer block, R. Zimmerman (RPG-Radiometer) for his excellent and hard work on the 780–870- and 982-GHz multipliers, J. Carlstrom for his enduring work on the 130–146-GHz Gunn oscillator, B. Weber and W. Schaal for their work on the 3-D modeling, M. Gould for his incredible overnight machining abilities, and lastly, author J. W. Kooi thanks his wife for her faithful support.

References

[1] B. N. Ellison and R. E. Miller, "A low noise 230 GHz SIS receiver," *Int. J. Infrared Millim. Waves*, vol. 8, pp. 609–625, 1987.

[2] A. R. Kerr, "An adjustable short-circuit for millimeter waveguides," Nat. Radio Astronomy Observatory, Charlottesville, VA, Electron. Div. Internal Rep. 280, July 1988.

[3] J. W. Kooi, C. K. Walker, H. G. LeDuc, T. R. Hunter, D. J. Benford, and T. G. Phillips, "A low noise 665 GHz SIS quasiparticle waveguide receiver," *Int. J. Infrared Millim. Waves*, vol. 15, no. 3, pp. 477–492, 1994.

[4] T. H. Büttgenbach, H. G. LeDuc, P. D. Maker, and T. G. Phillips, "A fixed tuned broadband matching structure for submillimeter receivers," *IEEE Trans. Appl. Superconduct.*, vol. 2, pp. 165–175, Sept. 1992.

[5] J. W. Kooi, M. Chan, B. Bumble, and T. G. Phillips, "A low noise 345 GHz waveguide receiver employing a tuned 0.50 μm^2 Nb/AlO$_x$/Nb

tunnel junction," *Int. J. Infrared Millim. Waves*, vol. 15, no. 5, pp. 783–805, May 1994.
[6] J. W. Kooi, M. Chan, B. Bumble, H. G. Leduc, P. L. Schaffer, and T. G. Phillips, "230 and 492 GHz low-noise SIS waveguide receivers employing tuned Nb/AlO_x/Nb tunnel junctions," *Int. J. Infrared Millim. Waves*, vol. 16, no. 12, pp. 2049–2068, Dec. 1995.
[7] C. K. Walker, J. W. Kooi, M. Chan, H. G. Leduc, P. L. Schaffer, J. E. Carlstrom, and T. G. Phillips, "A low-noise 492 GHz SIS waveguide receiver," *Int. J. Infrared Millim. Waves*, vol. 13, pp. 785–798, June 1992.
[8] S. Padin and G. Ortiz, "A cooled 1–2 GHz balanced HEMT amplifier," *IEEE Trans. Microwave Theory Tech.*, vol. 39, pp 1239–1243, July 1991.
[9] M. Salez, P. Febre, W. R. McGrath, B. Bumble, and H. G. LeDuc, "An SIS waveguide heterodyne receiver for 600 GHz–635 GHz," *Int. J. Infrared Millim. Waves*, vol. 15, no. 2, 349–368, Feb. 1994.
[10] P. Febre, W. R. McGrath, P. Batelaan, B. Bumble, H. G. LeDuc, S. George, and P. Featrier, "A low-noise SIS receiver measured from 480 GHz to 650 GHz using Nb junctions with integrated RF tuning circuits," *Intl. J. Infrared Millim. Waves*, vol. 15, no. 6, June 1994.
[11] J. W. Kooi, M. S. Chan, M. Bin, B. Bumble, H. G. Leduc, C. K. Walker, and T. G. Phillips, "The development of an 850 GHz waveguide receiver using tuned SIS junctions on 1 μm Si_3N_4 membranes," *Int. J. Infrared Millim. Waves*, vol. 16, no. 2, pp. 349–362, Feb. 1995.
[12] R. Pöpel, "Electromagnetic properties of superconductors," in *Superconducting Quantum Electronics*, V. Kos, Ed. Berlin, Germany: Springer-Verlag, 1989, pp. 44–78.
[13] R. Zimmerman, T. Rose, T. W. Crowe, and T. W. Grein, "An all-solid-state 1 THz radiometer for space applications," presented at the 6th Int. Symp. Space THz Technol., Pasadena, CA, Mar. 1995.
[14] J. W. Kooi, M. Chan, T. G. Phillips, B. Bumble, and H. G. Leduc, "A low noise 230 GHz heterodyne receiver employing 0.25 μm^2 area Nb/AlO_x/Nb tunnel junctions," *IEEE Trans. Microwave Theory Tech.*, vol. 40, pp. 812–815, May 1992.
[15] J. Zmuidzinas and H. G LeDuc, "Quasi-optical slot antenna SIS mixers," *IEEE Trans. Microwave Theory Tech.*, vol. 40, pp. 1797–1804, Sept. 1992.
[16] D. C. Mattis and J. Bardeen, "Theory of the anomalous skin effect in normal and superconducting metals," *Phys. Rev.*, vol 111, pp. 412–417, 1958.
[17] M. Bin, M. C. Gaidis, J. Zmuidzinas, T. G. Phillips, and H. G. LeDuc, "Quasi-Optical SIS mixer with Normal-Metal Tuning Strutures," *IEEE Trans. Appl. Superconduct.*, vol. 7, pp. 3584–3588, June 1997.
[18] M. Gurivch, M. A. Washington, and H. A. Huggins, "High quality refractory Josephson tunnel junction utilizing thin aluminum layers," *Appl. Phys. Lett.*, vol. 42, pp. 472–474, 1983.
[19] H. G. LeDuc, B. Bumble, S. R. Cypher, and J. A. Stern, in *2nd Int. Symp. Space THz Technol.*, Pasadena, CA, Feb. 1991, Feb. 26–28.
[20] J. R. Tucker and M. J. Feldman, "Quantum detection at millimeter wavelengths," *Rev. Mod. Phys.*, vol. 57, pp. 1055–1113, Oct. 1985.
[21] S. Rudner, M. J. Feldman, E. Kollberg, and T. Claeson, "Superconducting-insulator-superconducting mixing with arrays at millimeter-wave frequencies," *J. Appl. Phys.*, vol. 52, pp. 6366–6371, 1981.
[22] D. P. Woody, R. E. Miller, and M. J. Wengler, "85–115 GHz receivers for radio astronomy," *IEEE Trans. Microwave Theory Tech.*, vol. MTT-33, pp. 90–95, Feb. 1985.
[23] J. Lange, "Noise characterization of linear two ports in terms of invariant parameters," *IEEE J. Solid-State Circuits*, vol. SC-2, pp. 37–40, June 1967.
[24] A. Skalare, "Determining embedding circuit parameters from DC measurements on quasiparticles mixers," *Int. J. Inrared Millim. Waves*, vol. 10, pp. 1339–1353, 1989.
[25] N. B. Dubash, G. Pance, and M. J. Wengler, "Photon noise in the SIS detector," presented at the 4th Int. Symp. THz Technol., Los Angeles, CA, 1993.
[26] N. B. Dubash, M. J. Wengler, and J. Zmuidzinas, "Shot noise and photon-induced correlations in 500-GHz SIS detectors," *IEEE Trans. Appl. Superconduct.*, vol. 5, pp. 3308–3311, June 1995.
[27] M. J. Wengler and D. P. Woody, "Quantum noise in heterodyne detection," *IEEE J. Quantum Electron.*, vol. QE-23, pp. 613–622, May 1987.
[28] D. P. Woody, S. Padin, H. LeDuc, and J. Stern, "On using the shot noise in SIS tunnel junctions for characterizing IF amplifiers," presented at the *6th Int. Symp. Space THz Technol.*, Pasadena, CA, Mar. 21–23, 1995.
[29] R. Blundell, R. E. Miller, and K. H. Gundlach, "Understanding noise in SIS receivers," *Int. J. Infrared Millim. Waves*, vol. 13, no. 1, pp. 3–26, 1992.
[30] Q. Ke and M. J. Feldman, "A technique for noise measurements of SIS receivers," *IEEE Trans. Microwave Theory Tech.*, vol. 42, pp. 752–755, Apr. 1994.
[31] H. B. Callen and T. A. Welton, "Irreversibility and generalized noise," *Phys. Rev.*, vol. 83, no. 1, pp. 34–40, July 1951.
[32] A. R. Kerr, M. J. Feldman, and S. K. Pan, "Receiver noise temperature, the quantum noise limit, and the role of the zero-point fluctuations," Nat. Radio Astronomy Observatory, Charlottesville, VA, Electron. Div. Internal Rep. 304, Sept. 1996.
[33] D. Winkler and T. Claeson, "High frequency limits of superconducting tunnel junction mixers," *J. Appl. Phys.*, vol. 62, pp. 4482–4498, 1987.

Jacob W. Kooi was born in Geldrop, The Netherlands, on July 12, 1960. He received the B.S. degree in microwave engineering from the California Polytechnic State University, San Luis Obispo, in 1985, and the M.S. degree in electrical engineering from the California Institute of Technology, Pasadena, in 1992.

His research interests are in the area of millimeter- and submillimeter-wave technology and their applications.

Jérôme Pety was born in Lille, France, on June 27, 1970. He received the B.S. degree in physics from the Ecole Normale Superieure, Paris, France, in 1993, and is currently working toward the Ph.D. degree.

His research interests are in the area of superconducting devices and their application to submillimeter astronomy.

Bruce Bumble received the B.E. degree in engineering physics from Stevens Institute of Technology, Hoboken, NJ, in 1982 and the M.S. degree in materials science from the Polytechnic University of New York, Brooklyn, in 1989.

He is currently a Member of Technical Staff at the Jet Propulsion Laboratory, California Institute of Technology, Pasadena. His research interests include the field of superconducting device fabrication for radio astronomy applications.

Mr. Bumble has been a member of the American Vacuum Society for 14 years. He has participated in the Applied Superconductivity Conferences since 1986.

Christopher K. Walker was born in Shelby, N.C., on December 20, 1957. He received the B.S. in electrical engineering from Clemson University, Clemson, SC, in 1980, the M.S. degree in electrical engineering from Ohio State University, Athens, in 1981, and the Ph.D. degree in astronomy from the University of Arizona, Tucson, in 1988, where his thesis research was on protostellar evolution and radio astronomy instrumentation.

He then worked as a Microwave Engineer at TRW Areospace, Redondo Beach, CA, and the Jet Propulsion Laboratory, California Institute of Technology, Pasadena, from 1981 to 1983. While at Caltech, he continued his work in protostellar evolution. He then returned to the University of Arizona, as an Assistant Professor of astronomy, and is currently an Associate Professor of astronomy.

Dr. Walker was the recipient of a Millikan Fellowship in Physics from the California Institute of Technology.

Henry G. LeDuc was born in Butte, MT, on March 8, 1955. He received the B.S. degree in physics from Montana State University, Bozeman, in 1977, and the Ph.D. degree in physics from the University of California at Davis, in 1983. His thesis work involved far-IR spectroscopy of solid-state ionic conductors.

He is currently a Group Leader at the Jet Propulsion Laboratory, California Institute of Technology, Pasadena, where his group develops SIS tunnel junctions for heterodyne receivers.

P. L. Schaffer, photograph and biography not available at the time of publication.

T. G. Phillips, photograph and biography not available at the time of publication.